Heliyon 10 (2024) e29350

Contents lists available at ScienceDirect

Heliyon

journal homepage: www.cell.com/heliyon

Research article

Exploration of anatomical distribution of brain metastasis from breast cancer at first diagnosis assisted by artificial intelligence

Yi-min Han [a,1], Dan Ou [a,1], Wei-min Chai [b], Wen-lei Yang [c], Ying-long Liu [d], Ji-feng Xiao [d], Wei Zhang [e], Wei-xiang Qi [a,**], Jia-yi Chen [a,*]

[a] Department of Radiation Oncology, Ruijin Hospital, Shanghai Jiaotong University School of Medicine, Shanghai, China
[b] Department of Radiology, RuiJin Hospital, Shanghai Jiaotong University School of Medicine, Shanghai, China
[c] Department of Neurosurgery, RuiJin Hospital, Shanghai Jiaotong University School of Medicine, Shanghai, China
[d] United Imaging Research Institute of Innovative Medical Equipment, Shenzhen, China
[e] Shanghai United Imaging Healthcare Co., Ltd. Shanghai, China

ARTICLE INFO

Keywords:
Breast cancer
Brain metastasis
Molecular subtype
Anatomical distribution
Automatic segmentation

ABSTRACT

Objectives: This study aimed to explore the spatial distribution of brain metastases (BMs) from breast cancer (BC) and to identify the high-risk sub-structures in BMs that are involved at first diagnosis.

Methods: Magnetic resonance imaging (MRI) scans were retrospectively reviewed at our centre. The brain was divided into eight regions according to its anatomy and function, and the volume of each region was calculated. The identification and volume calculation of metastatic brain lesions were accomplished using an automatically segmented 3D BUC-Net model. The observed and expected rates of BMs were compared using 2-tailed proportional hypothesis testing.

Results: A total of 250 patients with BC who presented with 1694 BMs were retrospectively identified. The overall observed incidences of the substructures were as follows: cerebellum, 42.1 %; frontal lobe, 20.1 %; occipital lobe, 9.7 %; temporal lobe, 8.0 %; parietal lobe, 13.1 %; thalamus, 4.7 %; brainstem, 0.9 %; and hippocampus, 1.3 %. Compared with the expected rate based on the volume of different brain regions, the cerebellum, occipital lobe, and thalamus were identified as higher risk regions for BMs (P value $\leq 5.6*10^{-3}$). Sub-group analysis according to the type of BC indicated that patients with triple-negative BC had a high risk of involvement of the hippocampus and brainstem.

Conclusions: Among patients with BC, the cerebellum, occipital lobe and thalamus were identified as higher-risk regions than expected for BMs. The brainstem and hippocampus were high-risk areas of the BMs in triple negative breast cancer. However, further validation of this conclusion requires a larger sample size.

* Corresponding author. Department of Radiation Oncology, Ruijin Hospital, Shanghai Jiaotong University School of Medicine, 197 Ruijin Second Road, Shanghai, 200025, China.
** Corresponding author. Department of Radiation Oncology, Ruijin Hospital, Shanghai Jiaotong University School of Medicine, 197 Ruijin Second Road, Shanghai 200025, China.
E-mail addresses: hym11910@rjh.com.cn (Y.-m. Han), od12341@rjh.com.cn (D. Ou), cwm11394@rjh.com.cn (W.-m. Chai), yangwenlei@hotmail.com (W.-l. Yang), liuyinglong2014@163.com (Y.-l. Liu), jifeng.xiao@cri-united-imaging.com (J.-f. Xiao), wei.zhang01@united-imaging.com (W. Zhang), qwx12055@rjh.com.cn (W.-x. Qi), cjy11756@rjh.com.cn (J.-y. Chen).
[1] Yi-min Han and Dan Ou equally contributed to this work.

https://doi.org/10.1016/j.heliyon.2024.e29350
Received 20 December 2023; Received in revised form 3 April 2024; Accepted 5 April 2024
Available online 18 April 2024

List of abbreviations

BC	Breast cancer
BM(s)	Brain metastasis(es)
BCBM(s)	Breast cancer brain metastasis(es)
MRI	Magnetic resonance imaging
SRS	Stereotactic radiosurgery
HR	Hormone receptor
TNBC	Triple-negative breast cancer
MNI	Montreal Neurological Institute
AI	Artificial intelligence
DICE	Sørensen–Dice coefficient
3D-T1-FSPGR	Gadolinium-enhanced 3D-T1-fast spoiled gradient recalled echo
HA-WBRT	Hippocampal avoidance whole-brain radiation therapy
RTOG	Radiation Therapy Oncology Group
PFS	Progression-free survival
OS	Overall survival
KPS	Karnofsky performance status

1. Introduction

Breast cancer (BC) is the most common msalignancy in women in China [1,2]. The incidence of brain metastases (BMs) in patients with BC may increase due to improvements in imaging technologies and improved survival outcomes with novel anti-cancer treatments. It is estimated that approximately 5.1 % of patients with BC will develop BM [3]. Clinically, patients with BMs may suffer from motor, sensory, and cognitive dysfunctions. According to the National Comprehensive Cancer Network guidelines, current treatments for BMs include surgical resection, systematic therapy, radiation, and radiosurgery. Since the 1950s, intracranial radiotherapy has been used in the treatment of BMs [4]. With the continuous development of radiotherapy technology, advanced radiation therapy techniques such as stereotactic radiosurgery (SRS) and hippocampal avoidance whole-brain radiation therapy (HA-WBRT), are more frequently used in clinical treatment to protect patients' cognitive function and reduce radiation-related side effects. BC is classified into four subtypes based on its molecular features: hormone receptor (HR) -positive/human epidermal growth factor receptor 2 (HER2)-negative; HR-positive/HER2-positive; HR-negative/HER2-positive; and triple-negative breast cancer (TNBC). Previous studies have shown that HR-negative/HER2-positive tumours and TNBC are more likely to develop BMs [5] [–] [7]. Therefore, understanding the spatial distributions of BMs in BC subtypes and identifying the high-risk sub-structures of BMs would allow for more precise prophylactic irradiation strategies.

Magnetic resonance imaging (MRI) has become the standard method for determining the spatial distribution of BMs from primary BC. In addition, artificial intelligence (AI) has significantly improved the early detection of BMs. MRI is a commonly used non-invasive tool for brain disease detection and diagnosis; however, it is also time-consuming and labor-intensive. Recent advancements in machine learning and efficient computation have introduced a computer-assisted solution that rapidly and accurately analyses MRI images to identify anomalies. These computer-aided systems offer the potential to swiftly classify diseases for early treatment. Since 1998, computer experts have been attempting to automatically segment intracranial lesions on MRI using deep learning, and over 20 years, the algorithms have been continuously iterated and updated [8]. The invention of an automatic plotting system for BMs can promote accurate clinical diagnosis and therapy, as well as enhance the efficiency of image processing [9]. Related studies have indicated that exploring the spatial distribution characteristics of intracranial metastases through MRI is feasible [10]. Using MRI scans, Quattrocchi et al., revealed the non-uniform spatial distribution of BMs in patients with breast and lung cancers [11]. In recent years, a Korean study used this method to discover that BMs from HER2-positive and luminal types predominate in the occipital lobe and cerebellum, while those from TNBC predominate in the frontal lobe, limbic region, and parietal lobe [12]. However, a previous study indicated that the standardized registration image used by the Montreal Neurological Institute (MNI) 152 would lead to spatial mismatch in functional studies, especially at cortical regions the of superior and posterior brain when compared to the Chinese Brain Template [13]. In addition, the anatomical distribution of BMs from Chinese patients with BC remains unknown. Therefore, we performed this present study to analyse the spatial distribution of BMs from BC at initial diagnosis in a large patient database and to identify the high-risk sub-structures that BMs involved at first diagnosis, which might help us optimize the localized radiation treatment for patients with breast cancer brain metastasis (BCBM).

2. Materials and methods

2.1. Data source

This study utilised the outpatient and inpatient records of patients with BC who are admitted to our centre between January 2010 and July 2021. The dates of the initial BC and BM diagnoses were collected.

2.2. Patient population

This was a retrospective, observational study. The inclusion criteria were as follows: (1) patients with a confirmed diagnosis of BC;

(2) patients with a first-time diagnosis of BMs from BC and had no identification of BMs in previous brain MRI; and (3) those with at least one measurable lesion (diameter ≥3 mm) in the brain. The exclusion criteria were as follows: (1) intracranial treatment before MRI; (2) leptomeningeal invasion without parenchymal metastases; and (3) unknown or ambiguous pathological records. Our study began with the extraction of brain MRI data spanning a decade, targeting diagnoses indicative of BC-related intracranial pathology. The initial identification yielded a broad cohort that was meticulously refined through successive screenings for patients with confirmed intracranial solid tumours satisfying the specific inclusion criteria, leading to the final selection of female patients. Male patients (with one exception), those with non-breast primary tumours, and instances of inadequate imaging or prior intracranial

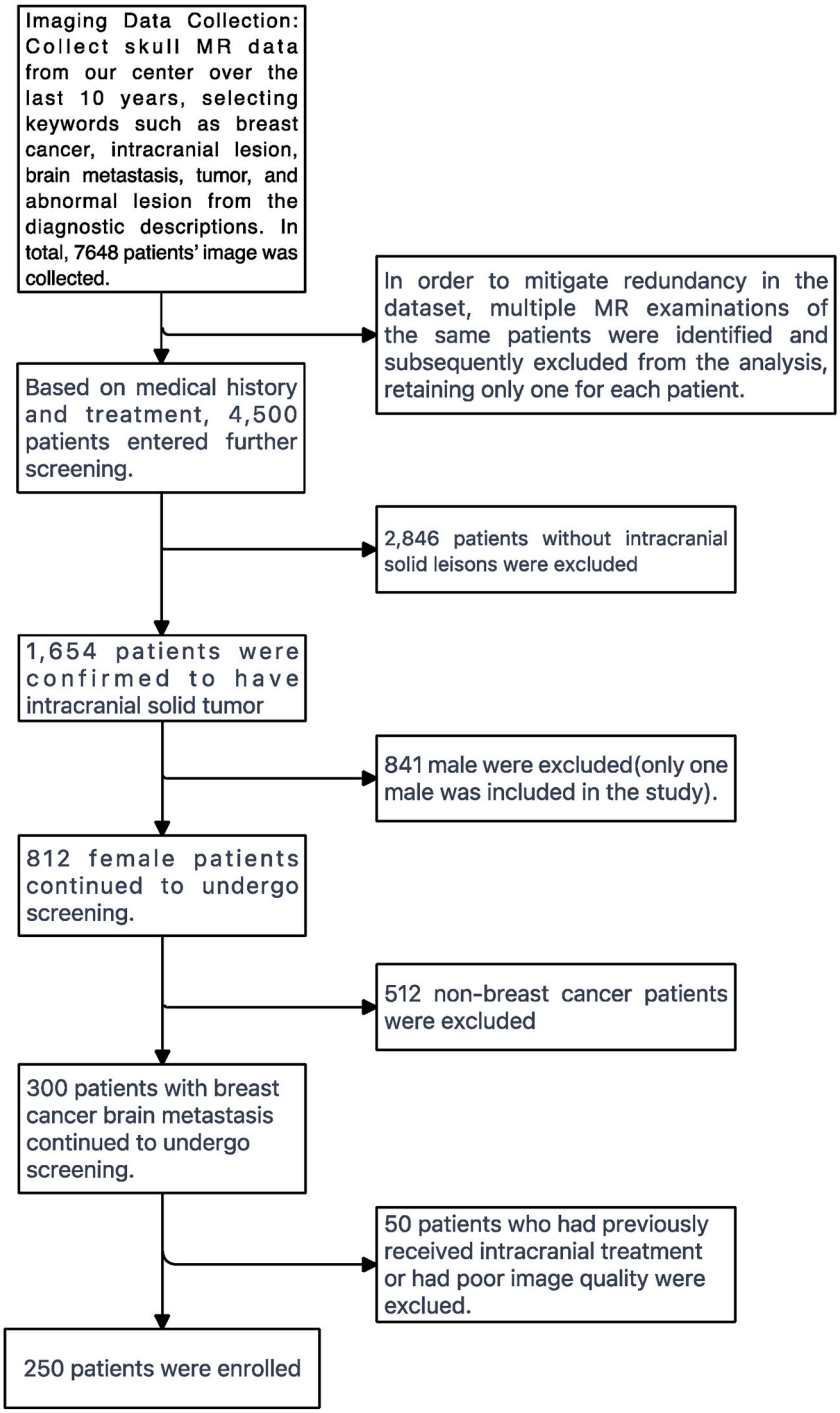

Fig. 1. Flowchart of patient screening for inclusion.

interventions were excluded. The detailed patient screening process is depicted in Fig. 1. The patients were divided into four groups according to their HR status and HER2 status. Based on the joint guidelines of the College of American Pathologists and the American Society of Clinical Oncology, ER-positive BC is typically defined as cases where at least 1 % of tumor cells express the ER [14]. Immunohistochemistry was used to assess ER, PR, and HER2 expression in primary BC. Fluorescence in situ hybridisation for HER2 amplification was performed in immunohistochemistry 2+ cases. Based on the HR and HER2 status, the patients were classified into HR-positive/HER2-negative, HR-positive/HER2-positive, HR-negative/HR-positive, and TNBC subtypes.

2.3. MRI protocol

The baseline characteristics of patients with BC and pre-treatment brain MRI images were obtained. A senior radiologist at our facility reviewed the Digital Imaging and Communications in Medicine gadolinium-enhanced 3D-T1-fast spoiled gradient recalled echo (3D-T1-FSPGR) sequence to determine the presence of BMs. After gathering the BM-containing MRI images, the physician workstation provided by United Imaging Healthcare Co., Ltd. Automatically segmented the BM lesions (www.united-imaging.com). The workstation algorithm for recognising tumour signals has been recognised [15,16]. The existing deep-learning-based segmentation model was used for the auto-segmentation of the whole brain tissue, which resulted in the removal of the skull from all MRI images. The algorithm and computer principles used by this software to identify intracranial metastatic tumours are provided in Supplementary Material 1.

To reduce the computational load of the network, all MRI sequences were cropped to include only regions with non-zero values. In Addition, to facilitate the proper learning of spatial semantics by the network, all MRI sequences were resampled to the median voxel spacing of the dataset. Third-order spline interpolation was used for the images of all MRI scans, and nearest-neighbour interpolation was used for their corresponding contours. Finally, all images were normalised using simple Z-score normalisation for the individual patients.

To increase the diversity of the data and address the overfitting problem caused by training a deep network with limited data, various real-time data enhancement techniques were employed. These techniques included random flipping, random zooming, random elastic deformation, gamma adjustment, and mirroring.

We manually verified the accuracy of these automatically segmented datasets. Lesions with a diameter of less than 2 mm had manually detected false-positive lesions, such as small blood vessels and holes, were excluded.

2.4. Validation of automatic segmentation accuracy

To validate the accuracy of the automatic segmentation software provided by United Imaging Healthcare Co., Ltd. for intracranial metastatic lesions, we obtained MRI images of another 20 patients with BCBM who had received intracranial radiotherapy at our centre between July 2021 and May 2023. We contoured the lesions both manually and by using the automatic segmentation software

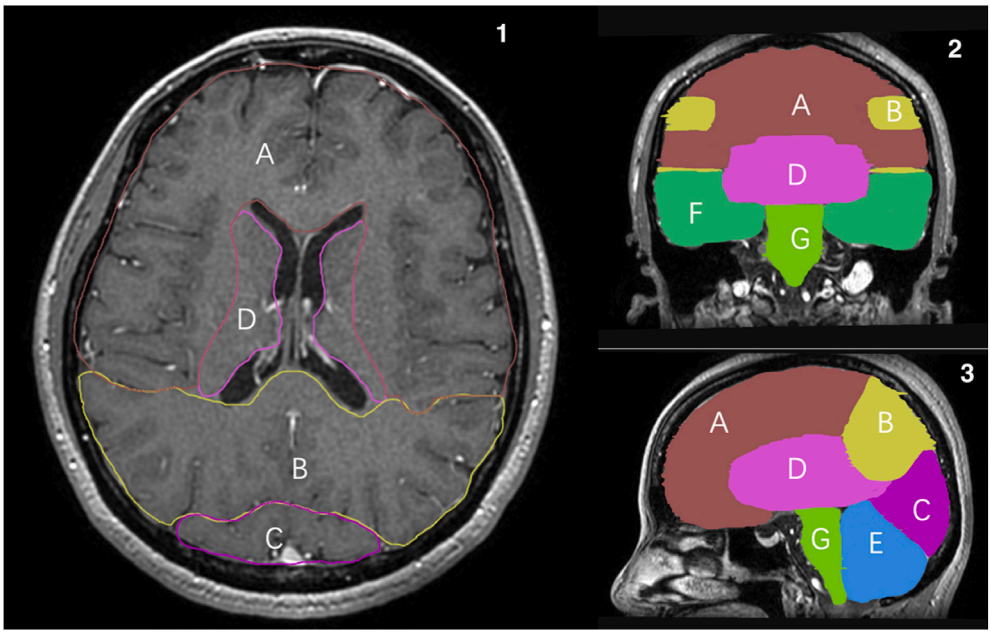

Fig. 2. The diagram illustrates schematic contouring of various brain regions. In the upper right corner, 1–3 respectively correspond to cross-section, coronal section, and sagittal section. A represents the frontal lobe, B represents the parietal lobe, C represents the occipital lobe, D represents the thalamus, E represents the cerebellum, F represents the temporal lobe, and G represents the brainstem.

to calculate its accuracy. After comparison, we found that the average Sørensen–Dice coefficient (DICE) value was 0.84 ± 0.08 and the Hausdorff 95 value was 2.25 ± 1.11, indicating a high precision of lesion identification (shown in Supplementary materials 2). Therefore, we believe that the automatically segmentation methods are reliable.

2.5. BMs analysis

We assumed that the risk of metastasis was the same for all parts of intracranial brain tissue. Therefore, we needed to measure the volume of each brain region and the proportion of tumor sites involved to analyse the spatial distribution and risk levels of BMs in different brain regions. The brain was divided into eight regions according to anatomy and function: the frontal lobe, temporal lobe, parietal lobe, occipital lobe, thalamus, brainstem, hippocampus, and cerebellum. A 3D-T1-FSPGR sequence was used to delineate brain lobes. We used computers to contour different brain regions on the cranial MRI scans of 250 patients. The specific contouring of each brain region is referred to as Gray's anatomy [17]. The hippocampal volume was measured using the Radiation Therapy Oncology Group (RTOG) 0933 contouring atlas [18,19]. Fig. 2 shows a schematic diagram of the contouring of different brain regions. After the contouring was completed, the computer automatically generated the volume of each region. We calculated the average value of each brain region for the 250 patients to obtain the volume of each brain region.

The diameter and volume of each BM on MRI were calculated slice-by-slice using the United Imaging Physician workstation. Tumour location was defined according to the following prelabelled anatomical structures in the brain: frontal, temporal, parietal, and occipital lobes; cerebellum; thalamus; hippocampus; and brainstem. In a few uncertain instances, tumours in the junctional zone were categorised according to the areas with greater volume involvement. To visualise the spatial distribution of BMs, we used the ITK-SNAP software (http://www.itksnap.org/) to merge all target delineations of each molecular type and display them as the main image. Fig. 3 shows the cross-sectional, sagittal, and coronal planes of the intracranial lesions using the ITK-SNAP tools.

2.6. Statistical analysis

The chi-square test was used to investigate the tumor sizes of the four molecular subgroups, the rate of involvement in various brain regions, and the number of BMs. Kaplan-Meier survival curve analysis was employed to assess the time interval from the initial diagnosis of primary BC to the development of BMs stratified by subtype. Statistical analyses were performed using SPSS software (IBM SPSS 19.0, SPSS Inc).

The observed rate of BMs in each brain region was estimated by dividing the number of BMs in that region by the total number of BMs in all the regions. Assuming an equal risk of metastasis from the BC for each voxel, the predicted rate of BMs in each brain area was determined by dividing the volume of each region by the total volume of all regions. To determine the probability of metastasis in each brain location, the actual and predicted rates of BMs were compared using 2-tailed proportional hypothesis testing as follows [20]:

$$Z = \frac{p - p_0}{\sqrt{\frac{p_0(1-p_0)}{n}}}$$

Annotation： p represents the observed rate of BMs, p_0 represents the expected rate of BMs, n represents the number of BMs, and Z represents the Z-score.

The cumulative probability of a normal distribution was used to figure out the Z-score's corresponding P value and the Bonferroni correction was used to account for the fact that many tests were performed across all anatomic ROIs. Therefore, the corrected significance level of P value was found by dividing the significance level of 0.05 by the number of ROIs, which was 8. The P value that was needed to reach statistical significance was $P \leq 6.25{*}10^{-3}$. In the brain regions with statistically significant P values, the areas of the brain with a positive or negative Z-score had a much higher or lower rate of BMs than expected.

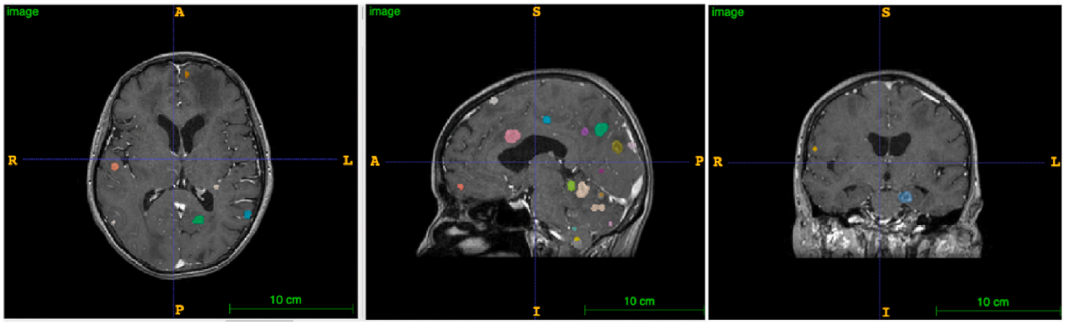

Fig. 3. The figure is a cross-sectional, sagittal, and coronal illustration of using Artificial Intelligence-assisted recognition to identify tumours. The parts shown in color in the figure are areas identified as tumours by Artificial Intelligence, and different colors are used to distinguish them for manual calculation. (For interpretation of the references to color in this figure legend, the reader is referred to the Web version of this article.)

3. Result

3.1. Patient characteristics

A total of 250 patients (249 females and one male)were included for analysis. No significant differences at baseline were detected among the four subtypes. The median time between primary tumor diagnosis and BMs was 40.9 months. Utilizing Kaplan-Meier survival curve analysis, we determined that the median duration from the initial diagnosis of primary BC to the onset of BM(s) stood at 56.2 months for patients with HR-positive BC. In contrast, HR-negative patients had a significantly shorter median time of 24.7 months (log-rank test, $P < 0.001$). For patients with HER2-positive BC, the median interval was 46.9 months, whereas their HER2-negative counterparts demonstrated a median time of 38.5 months, yielding no significant difference ($P = 0.741$). Baseline patient characteristics were summarized in Table 1.

3.2. Volume calculation segmentation of brain regions and overall BM distribution

Automated segmentation using the FastersuferCNN tool generated 78 brain areas. After integrating the substructures of the eight main brain areas, the following average brain volume was calculated: cerebellum 133.7 ± 12.8 cm^3, temporal lobe 204 ± 22.4 cm^3, occipital lobe 92 ± 7.5 cm^3, frontal lobe 510.6 ± 30.3 cm^3, parietal lobe 189.9 ± 15.8 cm^3, thalamus 20.1 ± 4.1 cm^3, brainstem 19.2 ± 1.6 cm^3, and hippocampus 10.2 ± 1.3 cm^3. The overall number of intracranial metastatic lesions among the different molecular subtypes is shown in Table 2.

The distribution and frequency of BMs are detailed in Table 3. There were a total of 1694 detectable lesions, including 101(40.4 %) patients diagnosed with single BM and 87 identified with multiple BMs (BMs ≥4). The overall observed incidences of the substructures were as follows: cerebellum, 42.1 % (714); temporal lobe, 8.0 % (136); occipital lobe, 9.7 % (165); frontal lobe, 20.1 % (341); parietal lobe, 13.1 % (222); thalamus, 4.7 % (79); brainstem, 0.9 % (15); and hippocampus, 1.3 % (22). The overall number of cases involving the eight brain regions was as follows: cerebellum, 57.2 % (143); temporal lobe, 17.2 % (43); occipital lobe, 16.8 % (42); frontal lobe, 30 % (75); parietal lobe, 20.4 % (51); thalamus, 9.2 % (23); brainstem, 3.6 % (9); and hippocampus, 3.6 % (9).

3.3. Distinctions between different molecular types

Table 4 outlines the features of BM in the four molecular subtypes of BC in the 250 patients. The HR-positive/HER2-positive subtype had a larger average tumour volume than the other three subtypes. The time from the diagnosis of BC or metastases to the BMs was shorter in HR-negative patients than in HR-positive patients($P < 0.05$). The proportions of supratentorial and infratentorial

Table 1
The baseline character of 250 patients.

Parameters	Number	Percentage (%)
Sex		
Female	249	99.6
male	1	0.4
Age		
≥60	101	40.4
< 60	149	59.6
Median	57	
Range	27–87	
Primary tumours		
IDC	239	95.6
DCIS	6	2.4
LCIS	3	1.2
MC	2	0.8
Molecular type		
HR-positive/HER-2-negative	80	32.0
HR-positive/HER-2-positive	45	18.0
HR-negative/HER-2-positive	55	22.0
TNBC	70	28.0
Extracranial metastases		
Yes	207	82.8
No	43	17.2
Extracranial tumor		
Stable	92	36.8
Active	158	63.2
BM status		
Synchronous	13	5.2
Metachronous	237	94.8
Clinical feature		
Symptomatic	215	86
Asymptomatic	35	14

Table 2
The number of brain metastases determined in various brain regions.

	HR-positive/HER-2-negative	HR-positive/HER-2-positive	HR-negative/HER-2-positive	TNBC	Total
Cerebellum	209	107	217	181	714
Temporal	24	13	54	45	136
Frontal	73	51	143	74	341
Occipital	50	21	54	40	165
Parietal	48	27	82	65	222
Brian stem	3	1	3	8	15
Thalamus	12	14	29	24	79
Hippocampus	5	2	5	10	22

Table 3
The statistical analysis of imaging comparison between different molecular types of brain metastases.

	HR-positive/HER-2-negative	HR-positive/HER-2-positive	HR-negative/HER-2-positive	TNBC	*P*-value
No of cases	80	45	55	70	
Average volume(cm^3)	8.39 ± 14.67	12.95 ± 17.43	13.7 ± 15.37	10.3 ± 13.38	0.045
Median time from first Time from the first metastasis to BM (months)	22.4	13.5	5.7	6.4	0.027
Median time from the diagnosis of BC to BM (months)	59.8	52.0	24.4	24.8	0.0003
Dura (n, %)	4(5)	1(2.2)	2(3.6)	3(4.3)	0.894
Leptomeningeal (n, %)	6(7.5)	0(0)	2(3.6)	2(2.9)	0.196
Supratentorial (n, %)	70(87.5)	35(77.8)	49(89.1)	60(85.7)	0.390
Infratentorial (n, %)	41(51.3)	21(46.7)	34(61.8)	47(67.1)	0.090
Supratentorial + Infratentorial (n, %)	43(53.8)	25(55.6)	43(78.2)	55(78.6)	0.001
Temporal lobe (n, %)	18(22.5)	9(20)	18(32.7)	22(31.4)	0.313
Occipital lobe (n, %)	27(33.8)	11(24.4)	22(40)	17(24.3)	0.223
Frontal lobe (n, %)	49(61.3)	22(48.9)	30(54.5)	31(44.3)	0.198
Parietal lobe (n, %)	30(37.5)	15(33.3)	23(41.8)	33(47.1)	0.646
Thalamus (n, %)	12(15)	7(15.6)	12(21.8)	13(18.6)	0.748
Brian stem (n, %)	3(3.8)	1(2.2)	3(5.5)	8(11.4)	0.136
Hippocampus (n, %)	5(6.3)	2(4.4)	5(9.1)	10(14.3)	0.227
Single metastasis (n, %)	24(30)	21(46.7)	20(36.4)	36(51.4)	0.041
No of BMs 1–3(n, %)	50(62.5)	32(71.1)	31(56.4)	50(71.4)	0.257
No of BMs ≥4(n, %)	30(37.5)	13(28.9)	24(43.6)	20(28.6)	

Table 4
Overall results of predicted and observed proportion of BMs in different brain regions.

Region	Volume, cm3	Expected rate (%)	No. observed	Observed Rate (%)	Z-score	*p* -value
Cerebellum	133.7	0.11	714	0.42	40.01	$2.81*10^{-314}$
Temporal lobe	204	0.17	136	0.08	−10.08	$6.53*10^{-24}$
Occipital lobe	92	0.08	165	0.09	2.98	$2.89*10^{-3}$
Frontal lobe	510.6	0.43	341	0.20	−19.24	$1.87*10^{-82}$
Parietal lobe	189.8	0.16	222	0.13	−3.34	$8.27*10^{-4}$
Thalamus	20.1	0.02	79	0.05	9.41	$4.87*10^{-21}$
Brain stem	19.2	0.02	15	0.01	−2.41	0.0159
Hippocampus	10.2	0.01	22	0.01	1.93	0.05368

Note: the corrected significance level of *P* value was calculated as the significance level 0.05 divided by 8 which was the number of ROIs, and the *P* value needed to reach statistical significance was $P \leq 6.25*10^{-3}$.

involvement were significantly higher in the HR-negative subtype than in the HR-positive subtype. Patients with TNBC had a higher risk of brainstem metastasis than those with the other three types (11.4 % vs. 3.3 %, $P = 0.012$). The proportion of single BM in patients with TNBC was higher than that in other patients (51.4 %, $P = 0.041$).

We evaluated lesion distribution within the four molecular subtypes based on the data reported in Table 2. In consideration of brain volume factor, the comparison of the overall observed and expected rates of BMs showed that the cerebellum, occipital lobe, and thalamus had a higher risk than expected and the temporal lobe, frontal lobe, and parietal lobe had a lower risk than expected ($P \leq 6.25*10^{-3}$). Although there was no statistical difference between the overall observation proportion and prediction proportion of the brainstem and hippocampus, according to the analysis of the prediction proportion of different molecular types, we found that the proportion of the TNBC type in the brainstem and hippocampus was significantly higher than that of the other three subtypes (Fig. 4).

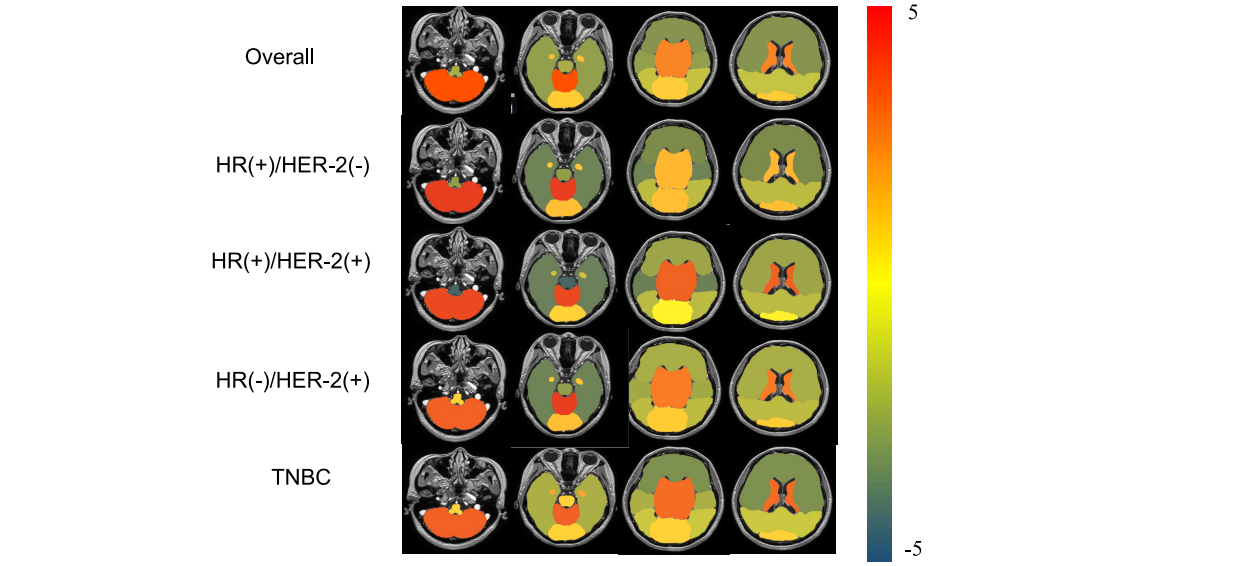

	Overall	HR(+)/HER-2(-)	HR(+)/HER-2(+)	HR(-)/HER-2(+)	Triple Negative
Cerebellum	3.72	4.33	4.00	3.27	3.59
Frontal lobe	2.15	3.04	3.14	1.88	1.71
Brian stem	1.25	1.46	1.14	1.18	1.15
Hippocampus	2.15	2.50	2.00	1.77	2.60
Occipital lobe	1.23	1.36	1.41	1.15	1.10
Temporal lobe	2.74	1.67	3.48	2.90	3.17
Parietal lobe	1.50	1.37	1.02	1.27	2.08
Thalamus	1.84	2.29	3.84	3.18	1.10

Fig. 4. The study examines the risk ratio of brain metastasis across different brain regions. This ratio is derived by dividing the observed ratio by the projected ratio. High-risk ratios are denoted by red, while low-risk ratios are denoted by blue. The values in the table beneath the figure represent the ratios of observed predicted values to actual observed values. Positive values indicate actual observed values exceeding predicted values, while negative values denote the inverse. (For interpretation of the references to color in this figure legend, the reader is referred to the Web version of this article.)

4. Discussion

To the best of our knowledge, this is the first large-scale study to assess the anatomical distribution of BMs in Chinese patients with BC at initial diagnosis. We retrospectively identified 250 patients with BC with 1694 measurable BMs for analysis using automatic segmentation. Prior to the present study, several studies compared the differences in intracranial distribution structures between BMs. Patients with lung cancer are more likely to develop BMs in the frontal and parietal lobes; however, patients with BC are more likely to have BM in the cerebellum and other areas with an abundance of nuclei [21,22]. Consistent with this finding, our results showed that the risk of developing BMs in the temporal, frontal, and parietal lobes was significantly lower than the expected rate, whereas the rate of BMs was higher in the occipital lobe, cerebellum, and thalamus. We then compared the characteristics of BMs according to BC subtypes and found that the time interval between the first diagnosis and the first BMs was shorter in HR-negative subtypes than in HR-positive subtypes, suggesting that HR-negative BC may have more aggressive intracranial metastasis. Similar results have been reported in previous studies [23]. The average tumour size in the HER2-positive BMs subtype was larger than those in the other three subtypes. In addition, TNBC has a higher chance of having a single metastasis at the time of initial diagnosis of BM. One possible explanation is that patients with TNBC with BM had shorter time intervals from primary diagnosis to brain involvement than HR-positive patients despite having mostly single lesions at initial detection. Moreover, the absence of effective therapy accelerates both systemic and intracranial disease progression in patients with TNBC, leading to worse outcomes than those in HR-positive patients.

Our findings may help to establish a more comprehensive survival prognostic model for BM. Classic Recursive Partitioning Analysis, established in 1997, stratifies patients into different prognostic groups based on age, Karnofsky Performance Status score, presence of extracranial metastases, and control of the primary tumour [24]. Subsequently, for BC, the Breast-Specific Graded Prognostic Assessment was established, which is a graded prognostic assessment model specific to BC that considers age, KPS, HER2 status, and extracranial metastatic sites [25]. In recent years, some new scoring criteria have been developed, such as a prediction

model based on postoperative disease-free survival and risk of BM, which considers age, tumour size, number of lymph node metastases, ER status, and Ki67 index. These scores include the patient's general condition, pathological information, and immunohistochemical results; imaging parameters are not included. With the current rapid development of multimodal imaging, imaging features can provide clinicians with useful information and predict the prognosis of patients. Therefore, by obtaining more detailed and complete data in the future, we can integrate patients' clinical, pathological, and imaging data and establish a more comprehensive survival prediction model. Subsequently, we compared the distribution pattern of BMs using intergroup analysis and demonstrated that the hippocampus and brainstem were more commonly involved in the TNBC subtype than in the other three subtypes. Currently, HA-WBRT has become the standard of care for patients without HA involvement who are planning to receive WBRT. Both the RTOG 0933 and NRG CC001 trials showed that HA-WBRT could better preserve cognitive function and decrease patient-reported symptoms, with no difference in intracranial progression-free survival (PFS) or overall survival (OS) when compared with WBRT [4,26]. Therefore, based on our findings, radiation oncologists should be cautious when recommending HA-WBRT for patients with TNBC.

Another important finding of our study was that 65.2 % of patients with an initial BMs diagnosis presented with 1–3 metastatic lesions, suggesting that most of the initial BMs from BC were limited. Therefore, stereotactic radiotherapy could be recommended for patients with BCs with BMs, as several large phase III trials have demonstrated that surgery or SRS in combination with whole brain radiotherapy could enhance the rate of intracranial disease control but did not improve OS [27] [–] [31]. The results of the N0574 clinical trial suggest that SRS alone could provide patients with a higher quality of life and more protection of neurocognitive function than SRS combined with WBRT [28]. Subsequent research demonstrated that SRS may be used for 1–10 BMs and is comparable to radiotherapy for the entire brain [32]. More than 85 % of the 250 people in the study had lesions with 10 metastases or less. This retrospective analysis revealed that most patients with BC and BMs are candidates for advanced stereotactic radiotherapy. These findings serve as a blueprint for future clinical studies. We plan to conduct extensive research and analysis on the treatment and survival of this patient population.

The median survival of patients with BC with BMs who did not receive any treatment was approximately 10 months [33]. Previous studies have shown that patients with TNBC and HER2-positive BC have shorter median survival times, whereas those with HR-positive BC have longer median survival times. A retrospective study of 1218 patients with stage II and III BC found that the median survival time after BM was 9, 13, and 17 months for patients with TNBC, HER2-positive, and HR-positive/HER2-negative tumours, respectively [34]. Another study also found that the median survival time after BM was 6.5, 10.5, and 11.5 months for patients with TNBC, HER2-positive, and HR-positive/HER2-negative BC, respectively [35]. In the era of targeted therapy, the median treatment time for HER2-positive patients has increased. A literature review of 4097 patients with BCBM found that the median survival time of HER2-positive patients receiving single or combined trastuzumab and lapatinib therapy was 18.9 months, whereas the median survival time of HER2-positive patients receiving other treatment regimens was 8.4–14.5 months [36]. The therapeutic efficacy of tucatinib in the management of cerebral metastases has been rigorously explored, yielding optimistic outcomes. Evidence derived from the HER2CLIMB study shows that the amalgamation of tucatinib with trastuzumab and capecitabine markedly enhances clinical results in individuals harbouring HER2-positive BC with cerebral dissemination. This pharmacological regimen has been shown to significantly diminish the hazard of cerebral progression or mortality by 68 % relative to the placebo cohort, registering a median central nervous system PFS of 9.9 months versus 4.2 months in the comparator group. Furthermore, an extension in OS was observed, with a 42 % decrease in mortality risk and a median OS of 18.1 months compared to 12.0 months in the placebo group. The intracranial objective response rate (ORR-IC) was substantially higher in the tucatinib cohort (47.3 %) than in the placebo arm (20.0 %) [37]. The updated analysis showed that nearly half of patients had BMs at baseline. The study found that the combination of tucatinib with trastuzumab and capecitabine significantly extended OS by 9.1 months compared to the placebo group. This combination also showed superior results in central nervous system progression-free survival, objective response rate in the intracranial compartment, and a longer duration of response. In addition, the risk of developing new brain lesions was notably reduced in the tucatinib group, highlighting its effectiveness in patients with HER2-positive metastatic BCBMs [38]. Prognostic differences in patients with BM across molecular subtypes may stem from treatment disparities and variations in intracranial tumour distribution. Our study indicates that TNBC is more prone to brainstem involvement, which is critical for vital physiological functions. This poses challenges in radiotherapy, necessitating a balance between delivering sufficient radiation to lesions without compromising the brainstem tissue and achieving suboptimal tumour control by reducing the dosage. This may also be one of the reasons why patients with TNBC have a worse prognosis after BM.

In this study, we investigated the application of deep learning algorithms in medical imaging analysis, focusing on their capability to automatically segment primary tumour volumes in MRI scans for BM radiotherapy. Employing the 3D U-Net Cascade architecture not only enhanced the segmentation accuracy and efficiency but also effectively addressed common challenges such as data imbalance and overfitting. Historically, algorithms used for the automatic segmentation of BMs primarily included deep-learning detection algorithms tailored for MRI images with contrast-enhanced black blood imaging data [39]. They employed a range of convolutional neural networks, such as the traditional U-Net, semiautomatic segmentation, and variants, which can automatically select lesion candidates and display them across multiple slices. Moreover, previous studies have utilised other deep learning models such as the DeepMedic neural network, which is capable of detecting and segmenting BMs within databases containing various MR sequences [40]. The 3D U-Net Cascade framework represents a significant advancement in the field of neuro-oncological imaging, providing an enhanced computational strategy for the automatic segmentation of cerebral metastatic lesions. This architecture is characterised by robust multiscale feature extraction, enabling detailed and granular analysis of neoplastic tissues. The iterative refinement techniques within the cascade ensure precision and significantly reduce the likelihood of segmentation errors. Moreover, the integration of complex volumetric data attributes and their intrinsic adaptability underscore their superiority in facilitating precision medicine in neuro-oncology. Previous studies have demonstrated that the 3D U-Net Cascade has achieved notable success in the automatic segmentation of condyles and hepatic tumours [41,42]. These findings provide a critical methodological foundation and insights for

further research and the application of deep learning technologies in medical imaging and related fields.

We did not employ the MNI 152 atlas used in other studies as a standard brain model [43,44]. This is because, at an early stage of the volume measurement effort, we discovered in the radiotherapy planning system that the volume of the intracranial substructure was significantly different from that of the same part of the MNI 152 atlas. For instance, the cerebellum volume cited in this paper was 294.6 cm^3, which is significantly greater than the cerebellar volume we outlined [44]. We consider this a distinction between ethnic groups; the MNI 152 collected 150 MRI volume images from a normative white young adult population, which may be different from information regarding Asian women. In addition, MNI 152 used T1-weighted images while we sued 3D-T1-FSPGR weighted images, which are thinner than T1-weighted images and provided a sharper depiction of the substructure. Using a radiotherapy planning system, we measured the volumes of different regions of the patient's MRI, which improved the objectivity of our results. Another strength of the present study is that we used AI contouring to identify the BMs. We performed external validation using a small-sample dataset and found that this model contoured intracranial lesions with a DICE value of 0.84 ± 0.08 and a Hausdorff 95 of 2.25 ± 1.11, which had better delineation accuracy than previous literature [45]. By applying AI, we can determine the number and volume of tumours faster and more accurately, although the current automatic identification function is limited and often regards small blood vessels, lacunar lesions, and other lesions smaller than 3 mm as BMs. The computer algorithms will be further updated to improve the automatic identification functions of the software.

Our study had several limitations. First, the risk of intracranial brain parenchymal lesions metastases might be associated with brain vascular supply, which need to be further explored. Second, an evaluation of the long-term clinical outcomes and survival prognosis for patients with BMs was not included in the study. This aspect is crucial, as it could provide valuable insights into disease progression, treatment effectiveness, and potential factors influencing patient survival. In addition, we duly acknowledge the presence of other limitations in our study such as the extracranial status assessment and a relatively low number of cases within each BC subtype and specific brain regions, which may affect the generalisability of our findings.

5. Conclusion

The temporal, frontal, and the parietal lobes demonstrated a low risk of BMs, while the cerebellar lobe was at a high risk of BMs in all types of BC. TNBC is more likely to involve the hippocampus and brainstem than the other three types of BC. Additionally, the relatively poorer prognosis observed in patients with TNBC following the development of BMs compared with other subtypes may be attributed to this factor. Further validation using a larger sample size is warranted to confirm these findings.

Ethical approval statement

This study received approval from the Ethics Committee of Ruijin Hospital, affiliated with the School of Medicine at Shanghai Jiao Tong University. The approval number for this study is (2020) Clinical Ethics Review No. 298 and performed in accordance with the Declaration of Helsinki. The Ethics Committee waived the requirement for informed consent from each participant.

Data availability statement

Clinical data were not publicly available due to involving patient privacy, but can be accessed from the author Yi-min Han (E-mail: hym11910@rjh.com.cn).

Funding

This study was supported in part by the National Key Research and Development Program of China (grant numbers 2016YFC0105409 and 2022YFC2404602), the Scientific and Technological Innovation Action Plan of the Shanghai Science and Technology Committee (grant number 22Y31900103) and complied with ethical standards.

CRediT authorship contribution statement

Yi-min Han: Writing – original draft, Resources, Methodology, Investigation, Formal analysis, Data curation. **Dan Ou:** Writing – original draft, Validation, Resources. **Wei-min Chai:** Visualization, Validation. **Wen-lei Yang:** Visualization, Validation. **Ying-long Liu:** Software, Methodology. **Ji-feng Xiao:** Software. **Wei Zhang:** Project administration. **Wei-xiang Qi:** Writing – review & editing, Methodology, Conceptualization. **Jia-yi Chen:** Supervision, Project administration, Conceptualization.

Declaration of competing interest

The authors declare that they have no known competing financial interests or personal relationships that could have appeared to influence the work reported in this paper.

Acknowledgements

The authors thank Professor Jia-yi Chen for her guidance and support. The authors also thank their colleagues at Shanghai United

Imaging Healthcare Co., Ltd. for their support and help in automatically segmenting brain volume and AI recognition of BMs. The authors would also like to thank Wei-min Chai, Director of the Radiology Department of our hospital, and Dr. Yang, Neurosurgery Department, for their theoretical support.

Appendix A. Supplementary data

Supplementary data to this article can be found online at https://doi.org/10.1016/j.heliyon.2024.e29350.

References

[1] R. Zheng, S. Zhang, H. Zeng, S. Wang, K. Sun, R. Chen, L. Li, W. Wei, J. He, Cancer incidence and mortality in China, 2016, Journal of the National Cancer Center 2 (2022) 1–9, https://doi.org/10.1016/j.jncc.2022.02.002.
[2] H. Sung, J. Ferlay, R.L. Siegel, M. Laversanne, I. Soerjomataram, A. Jemal, F. Bray, Global cancer statistics 2020: GLOBOCAN estimates of incidence and mortality worldwide for 36 cancers in 185 countries, CA Cancer J Clin 71 (2021) 209–249, https://doi.org/10.3322/caac.21660.
[3] J.S. Barnholtz-Sloan, A.E. Sloan, F.G. Davis, F.D. Vigneau, P. Lai, R.E. Sawaya, Incidence proportions of brain metastases in patients diagnosed (1973 to 2001) in the metropolitan Detroit cancer surveillance system, J. Clin. Oncol. 22 (2004) 2865–2872, https://doi.org/10.1200/JCO.2004.12.149.
[4] V. Gondi, S.L. Pugh, W.A. Tome, C. Caine, B. Corn, A. Kanner, H. Rowley, V. Kundapur, A. DeNittis, J.N. Greenspoon, A.A. Konski, G.S. Bauman, S. Shah, W. Shi, M. Wendland, L. Kachnic, M.P. Mehta, Preservation of memory with conformal avoidance of the hippocampal neural stem-cell compartment during whole-brain radiotherapy for brain metastases (RTOG 0933): a phase II multi-institutional trial, J. Clin. Oncol. 32 (2014) 3810–3816, https://doi.org/10.1200/JCO.2014.57.2909.
[5] V. Venur, J. Leone, Targeted therapies for brain metastases from breast cancer, Int. J. Mol. Sci. 17 (2016) 1543, https://doi.org/10.3390/ijms17091543.
[6] I. Witzel, L. Oliveira-Ferrer, K. Pantel, V. Müller, H. Wikman, Breast cancer brain metastases: biology and new clinical perspectives, Breast Cancer Res. 18 (2016) 8, https://doi.org/10.1186/s13058-015-0665-1.
[7] M.A. Kaplan, A. Isikdogan, D. Koca, M. Kucukoner, O. Gumusay, R. Yildiz, A. Dayan, L. Demir, C. Geredeli, M. Kocer, U.Y. Arslan, A. İnal, O.U. Unal, A.G. Mert, M. Bilici, M. Ozkan, E.T. Elkiran, S. Yaman, A.G. Durnalı, A. Suner, S. Alici, M.O. Tarhan, C. Boruban, Z. Urakci, S. Buyukberber, Biological subtypes and survival outcomes in breast cancer patients with brain metastases (study of the anatolian society of medical Oncology), Oncology 83 (2012) 141–150, https://doi.org/10.1159/000338782.
[8] T.A. Soomro, L. Zheng, A.J. Afifi, A. Ali, S. Soomro, M. Yin, J. Gao, Image segmentation for MR brain tumor detection using machine learning: a review, IEEE Rev Biomed Eng 16 (2023) 70–90, https://doi.org/10.1109/RBME.2022.3185292.
[9] D. Sikpa, J.P. Fouquet, R. Lebel, P. Diamandis, M. Richer, M. Lepage, Automated detection and quantification of breast cancer brain metastases in an animal model using democratized machine learning tools, Sci. Rep. 9 (2019) 17333, https://doi.org/10.1038/s41598-019-53911-x.
[10] Y. Wang, W. Xia, B. Liu, L. Zhou, M. Ni, R. Zhang, J. Shen, Y. Bai, G. Weng, S. Yuan, X. Gao, Exploration of spatial distribution of brain metastasis from small cell lung cancer and identification of metastatic risk level of brain regions: a multicenter, retrospective study, Cancer Imag. 21 (2021) 41, https://doi.org/10.1186/s40644-021-00410-w.
[11] C.C. Quattrocchi, Y. Errante, C. Gaudino, C.A. Mallio, A. Giona, D. Santini, G. Tonini, B.B. Zobel, Spatial brain distribution of intra-axial metastatic lesions in breast and lung cancer patients, J. Neuro Oncol. 110 (2012) 79–87, https://doi.org/10.1007/s11060-012-0937-x.
[12] S. Kyeong, Y.J. Cha, S.G. Ahn, S.H. Suh, E.J. Son, S.J. Ahn, Subtypes of breast cancer show different spatial distributions of brain metastases, PLoS One 12 (2017) e0188542, https://doi.org/10.1371/journal.pone.0188542.
[13] Tun Jao, Chun-Yuan Chang, Chia-Wei Li, Der-Yow Chen, E. Wu, Chang-Wei Wu, Chi-Hsuan Tsou, Chien-Chang Ho, Jyh-Horng Chen, Development of NTU standard Chinese brain template: morphologic and functional comparison with MNI template using magnetic resonance imaging, in: 2009 Annual International Conference of the, IEEE Engineering in Medicine and Biology Society, IEEE, 2009, pp. 4779–4782, https://doi.org/10.1109/IEMBS.2009.5334211.
[14] K.H. Allison, M.E.H. Hammond, M. Dowsett, S.E. McKernin, L.A. Carey, P.L. Fitzgibbons, D.F. Hayes, S.R. Lakhani, M. Chavez-MacGregor, J. Perlmutter, C. M. Perou, M.M. Regan, D.L. Rimm, W.F. Symmans, E.E. Torlakovic, L. Varella, G. Viale, T.F. Weisberg, L.M. McShane, A.C. Wolff, Estrogen and progesterone receptor testing in breast cancer: ASCO/CAP guideline update, J. Clin. Oncol. 38 (2020) 1346–1366, https://doi.org/10.1200/JCO.19.02309.
[15] F. Shi, W. Hu, J. Wu, M. Han, J. Wang, W. Zhang, Q. Zhou, J. Zhou, Y. Wei, Y. Shao, Y. Chen, Y. Yu, X. Cao, Y. Zhan, X.S. Zhou, Y. Gao, D. Shen, Deep learning empowered volume delineation of whole-body organs-at-risk for accelerated radiotherapy, Nat. Commun. 13 (2022) 6566, https://doi.org/10.1038/s41467-022-34257-x.
[16] S. Tian, C. Wang, R. Zhang, Z. Dai, L. Jia, W. Zhang, J. Wang, Y. Liu, Transfer learning-based autosegmentation of primary tumor volumes of glioblastomas using preoperative MRI for radiotherapy treatment, Front. Oncol. 12 (2022), https://doi.org/10.3389/fonc.2022.856346.
[17] Susan Standring, Gray's Anatomy:The Anatomical Basis of Clinical Practice, 39th ed., Churchill Livingstone, 2004.
[18] A. Ghia, W.A. Tomé, S. Thomas, G. Cannon, D. Khuntia, J.S. Kuo, M.P. Mehta, Distribution of brain metastases in relation to the Hippocampus: implications for neurocognitive functional preservation, Int. J. Radiat. Oncol. Biol. Phys. 68 (2007) 971–977, https://doi.org/10.1016/j.ijrobp.2007.02.016.
[19] V. Gondi, R. Tolakanahalli, M.P. Mehta, D. Tewatia, H. Rowley, J.S. Kuo, D. Khuntia, W.A. Tomé, Hippocampal-sparing whole-brain radiotherapy: a "how-to" technique using helical tomotherapy and linear accelerator–based intensity-modulated radiotherapy, Int. J. Radiat. Oncol. Biol. Phys. 78 (2010) 1244–1252, https://doi.org/10.1016/j.ijrobp.2010.01.039.
[20] T.K. Yanagihara, A. Lee, T.J.C. Wang, Quantitative analysis of the spatial distribution of metastatic brain lesions, Tomography 3 (2017) 16–22, https://doi.org/10.18383/j.tom.2016.00268.
[21] S. Kyeong, Y.J. Cha, S.G. Ahn, S.H. Suh, E.J. Son, S.J. Ahn, Subtypes of breast cancer show different spatial distributions of brain metastases, PLoS One 12 (2017) e0188542, https://doi.org/10.1371/journal.pone.0188542.
[22] C.C. Quattrocchi, Y. Errante, C. Gaudino, C.A. Mallio, A. Giona, D. Santini, G. Tonini, B.B. Zobel, Spatial brain distribution of intra-axial metastatic lesions in breast and lung cancer patients, J. Neuro Oncol. 110 (2012) 79–87, https://doi.org/10.1007/s11060-012-0937-x.
[23] I.A. Molnár, B.Á. Molnár, L. Vízkeleti, K. Fekete, J. Tamás, P. Deák, C. Szundi, B. Székely, J. Moldvay, S. Vári-Kakas, M.A. Szász, B. Ács, J. Kulka, A.-M. Tőkés, Breast carcinoma subtypes show different patterns of metastatic behavior, Virchows Arch. 470 (2017) 275–283, https://doi.org/10.1007/s00428-017-2065-7.
[24] C. Nieder, K. Marienhagen, S.T. Astner, M. Molls, Prognostic scores in brain metastases from breast cancer, BMC Cancer 9 (2009) 105, https://doi.org/10.1186/1471-2407-9-105.
[25] M.D. Hackshaw, H.E. Danysh, M. Henderson, E. Wang, N. Tu, Z. Islam, A. Ladner, M.E. Ritchey, M. Salas, Prognostic factors of brain metastasis and survival among HER2-positive metastatic breast cancer patients: a systematic literature review, BMC Cancer 21 (2021) 967, https://doi.org/10.1186/s12885-021-08708-5.
[26] P.D. Brown, V. Gondi, S. Pugh, W.A. Tome, J.S. Wefel, T.S. Armstrong, J.A. Bovi, C. Robinson, A. Konski, D. Khuntia, D. Grosshans, T.L.S. Benzinger, D. Bruner, M.R. Gilbert, D. Roberge, V. Kundapur, K. Devisetty, S. Shah, K. Usuki, B.M. Anderson, B. Stea, H. Yoon, J. Li, N.N. Laack, T.J. Kruser, S.J. Chmura, W. Shi, S. Deshmukh, M.P. Mehta, L.A. Kachnic, Hippocampal avoidance during whole-brain radiotherapy plus memantine for patients with brain metastases: phase III trial NRG Oncology CC001, J. Clin. Oncol. 38 (2020) 1019–1029, https://doi.org/10.1200/JCO.19.02767.

[27] M. Kocher, R. Soffietti, U. Abacioglu, S. Villà, F. Fauchon, B.G. Baumert, L. Fariselli, T. Tzuk-Shina, R.-D. Kortmann, C. Carrie, M. Ben Hassel, M. Kouri, E. Valeinis, D. van den Berge, S. Collette, L. Collette, R.-P. Mueller, Adjuvant whole-brain radiotherapy versus observation after radiosurgery or surgical resection of one to three cerebral metastases: results of the EORTC 22952-26001 study, J. Clin. Oncol. 29 (2011) 134–141, https://doi.org/10.1200/JCO.2010.30.1655.

[28] A.M. Hong, G.B. Fogarty, K. Dolven-Jacobsen, B.H. Burmeister, S.N. Lo, L.E. Haydu, J.L. Vardy, A.K. Nowak, H.M. Dhillon, T. Ahmed, B. Shivalingam, G.V. Long, A.M. Menzies, G. Hruby, K.J. Drummond, C. Mandel, M.R. Middleton, C.H. Reisse, E.J. Paton, V. Steel, N.C. Williams, R.A. Scolyer, R.L. Morton, J.F. Thompson, Adjuvant whole-brain radiation therapy compared with observation after local treatment of melanoma brain metastases: a multicenter, randomized phase III trial, J. Clin. Oncol. 37 (2019) 3132–3141, https://doi.org/10.1200/JCO.19.01414.

[29] H. Aoyama, H. Shirato, M. Tago, K. Nakagawa, T. Toyoda, K. Hatano, M. Kenjyo, N. Oya, S. Hirota, H. Shioura, E. Kunieda, T. Inomata, K. Hayakawa, N. Katoh, G. Kobashi, Stereotactic radiosurgery plus whole-brain radiation therapy vs stereotactic radiosurgery alone for treatment of brain metastases, JAMA 295 (2006) 2483, https://doi.org/10.1001/jama.295.21.2483.

[30] E.L. Chang, J.S. Wefel, K.R. Hess, P.K. Allen, F.F. Lang, D.G. Kornguth, R.B. Arbuckle, J.M. Swint, A.S. Shiu, M.H. Maor, C.A. Meyers, Neurocognition in patients with brain metastases treated with radiosurgery or radiosurgery plus whole-brain irradiation: a randomised controlled trial, Lancet Oncol. 10 (2009) 1037–1044, https://doi.org/10.1016/S1470-2045(09)70263-3.

[31] P.D. Brown, K. Jaeckle, K.V. Ballman, E. Farace, J.H. Cerhan, S.K. Anderson, X.W. Carrero, F.G. Barker, R. Deming, S.H. Burri, C. Ménard, C. Chung, V. W. Stieber, B.E. Pollock, E. Galanis, J.C. Buckner, A.L. Asher, Effect of radiosurgery alone vs radiosurgery with whole brain radiation therapy on cognitive function in patients with 1 to 3 brain metastases, JAMA 316 (2016) 401, https://doi.org/10.1001/jama.2016.9839.

[32] M. Yamamoto, T. Serizawa, T. Shuto, A. Akabane, Y. Higuchi, J. Kawagishi, K. Yamanaka, Y. Sato, H. Jokura, S. Yomo, O. Nagano, H. Kenai, A. Moriki, S. Suzuki, Y. Kida, Y. Iwai, M. Hayashi, H. Onishi, M. Gondo, M. Sato, T. Akimitsu, K. Kubo, Y. Kikuchi, T. Shibasaki, T. Goto, M. Takanashi, Y. Mori, K. Takakura, N. Saeki, E. Kunieda, H. Aoyama, S. Momoshima, K. Tsuchiya, Stereotactic radiosurgery for patients with multiple brain metastases (JLGK0901): a multi-institutional prospective observational study, Lancet Oncol. 15 (2014) 387–395, https://doi.org/10.1016/S1470-2045(14)70061-0.

[33] Q. Chen, J. Xiong, Y. Ma, J. Wei, C. Liu, Y. Zhao, Systemic treatments for breast cancer brain metastasis, Front. Oncol. 12 (2023), https://doi.org/10.3389/fonc.2022.1086821.

[34] T.Q. Cao, K. Dixit, C. Santa-Maria, P. Kumthekar, Factors affecting time to brain metastases for stage 2 and 3 breast cancer patients: a large single-institutional analysis with potential screening implications, Neurooncol Adv 3 (2021), https://doi.org/10.1093/noajnl/vdab009.

[35] Q. Liu, X. Kong, Z. Wang, X. Wang, W. Zhang, B. Ai, R. Gao, Y. Fang, J. Wang, NCCBM, a nomogram prognostic model in breast cancer patients with brain metastasis, Front. Oncol. 11 (2021), https://doi.org/10.3389/fonc.2021.642677.

[36] M.D. Hackshaw, H.E. Danysh, M. Henderson, E. Wang, N. Tu, Z. Islam, A. Ladner, M.E. Ritchey, M. Salas, Prognostic factors of brain metastasis and survival among HER2-positive metastatic breast cancer patients: a systematic literature review, BMC Cancer 21 (2021) 967, https://doi.org/10.1186/s12885-021-08708-5.

[37] N.U. Lin, V. Borges, C. Anders, R.K. Murthy, E. Paplomata, E. Hamilton, S. Hurvitz, S. Loi, A. Okines, V. Abramson, P.L. Bedard, M. Oliveira, V. Mueller, A. Zelnak, M.P. DiGiovanna, T. Bachelot, A.J. Chien, R. O'Regan, A. Wardley, A. Conlin, D. Cameron, L. Carey, G. Curigliano, K. Gelmon, S. Loibl, J. Mayor, S. McGoldrick, X. An, E.P. Winer, Intracranial efficacy and survival with tucatinib plus trastuzumab and capecitabine for previously treated HER2-positive breast cancer with brain metastases in the HER2CLIMB trial, J. Clin. Oncol. 38 (2020) 2610–2619, https://doi.org/10.1200/JCO.20.00775.

[38] N.U. Lin, R.K. Murthy, V. Abramson, C. Anders, T. Bachelot, P.L. Bedard, V. Borges, D. Cameron, L.A. Carey, A.J. Chien, G. Curigliano, M.P. DiGiovanna, K. Gelmon, G. Hortobagyi, S.A. Hurvitz, I. Krop, S. Loi, S. Loibl, V. Mueller, M. Oliveira, E. Paplomata, M. Pegram, D. Slamon, A. Zelnak, J. Ramos, W. Feng, E. Winer, Tucatinib vs placebo, both in combination with trastuzumab and capecitabine, for previously treated ERBB2 (HER2)-Positive metastatic breast cancer in patients with brain metastases, JAMA Oncol. 9 (2023) 197, https://doi.org/10.1001/jamaoncol.2022.5610.

[39] H. Jara, M.A. Barish, Black-blood MR angiography. Techniques, and clinical applications, Magn Reson Imaging Clin N Am 7 (1999) 303–317.

[40] A. Wadhwa, A. Bhardwaj, V. Singh Verma, A review on brain tumor segmentation of MRI images, Magn. Reson. Imaging 61 (2019) 247–259, https://doi.org/10.1016/j.mri.2019.05.043.

[41] N. Jha, T. Kim, S. Ham, S.-H. Baek, S.-J. Sung, Y.-J. Kim, N. Kim, Fully automated condyle segmentation using 3D convolutional neural networks, Sci. Rep. 12 (2022) 20590, https://doi.org/10.1038/s41598-022-24164-y.

[42] Y. Wu, H. Shen, Y. Tan, Y. Shi, Automatic liver tumor segmentation used the cascade multi-scale attention architecture method based on 3D U-Net, Int. J. Comput. Assist. Radiol. Surg. 17 (2022) 1915–1922, https://doi.org/10.1007/s11548-022-02653-9.

[43] S. Kyeong, Y.J. Cha, S.G. Ahn, S.H. Suh, E.J. Son, S.J. Ahn, Subtypes of breast cancer show different spatial distributions of brain metastases, PLoS One 12 (2017) e0188542, https://doi.org/10.1371/journal.pone.0188542.

[44] Y. Wang, W. Xia, B. Liu, L. Zhou, M. Ni, R. Zhang, J. Shen, Y. Bai, G. Weng, S. Yuan, X. Gao, Exploration of spatial distribution of brain metastasis from small cell lung cancer and identification of metastatic risk level of brain regions: a multicenter, retrospective study, Cancer Imag. 21 (2021) 41, https://doi.org/10.1186/s40644-021-00410-w.

[45] D.G. Hsu, Å. Ballangrud, A. Shamseddine, J.O. Deasy, H. Veeraraghavan, L. Cervino, K. Beal, M. Aristophanous, Automatic segmentation of brain metastases using T1 magnetic resonance and computed tomography images, Phys. Med. Biol. 66 (2021) 175014, https://doi.org/10.1088/1361-6560/ac1835.